J|A|C|S
JOURNAL OF THE AMERICAN CHEMICAL SOCIETY
pubs.acs.org/JACS

Article

Pressure-Modulated Anomalous Organic−Inorganic Interactions Enhance Structural Distortion and Second-Harmonic Generation in $MHyPbBr_3$ Perovskite

Yuhong Mao,[#] Songhao Guo,[#] Xu Huang, Kejun Bu, Zhongyang Li, Phuong Q. H. Nguyen, Gang Liu, Qingyang Hu, Dongzhou Zhang, Yongping Fu, Wenge Yang,* and Xujie Lü*

Cite This: J. Am. Chem. Soc. 2023, 145, 23842−23848

Read Online

ACCESS | Metrics & More | Article Recommendations | Supporting Information

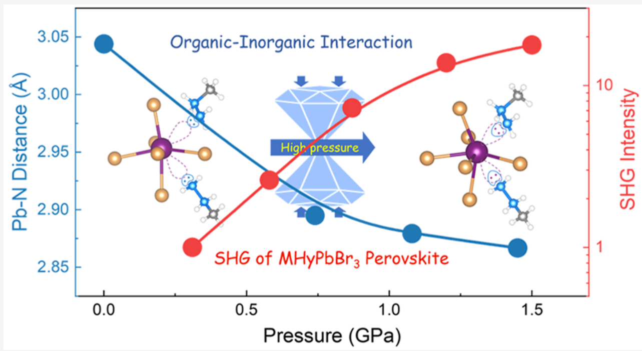

ABSTRACT: Organic−inorganic halide perovskites possess unique electronic configurations and high structural tunability, rendering them promising for photovoltaic and optoelectronic applications. Despite significant progress in optimizing the structural characteristics of the organic cations and inorganic framework, the role of organic−inorganic interactions in determining the structural and optical properties has long been underappreciated and remains unclear. Here, by employing pressure tuning, we realize continuous regulation of organic−inorganic interactions in a lead halide perovskite, $MHyPbBr_3$ (MHy^+ = methylhydrazinium, $CH_3NH_2NH_2^+$). Compression enhances the organic−inorganic interactions by strengthening the Pb−N coordinate bonding and N−H···Br hydrogen bonding, which results in a higher structural distortion in the inorganic framework. Consequently, the second-harmonic-generation (SHG) intensity experiences an 18-fold increase at 1.5 GPa, and the order−disorder phase transition temperature of $MHyPbBr_3$ increases from 408 K under ambient pressure to 454 K at the industrially achievable level of 0.5 GPa. Further compression triggers a sudden non-centrosymmetric to centrosymmetric phase transition, accompanied by an anomalous bandgap increase by 0.44 eV, which stands as the largest boost in all known halide perovskites. Our findings shed light on the intricate correlations among organic−inorganic interactions, octahedral distortion, and SHG properties and, more broadly, provide valuable insights into structural design and property optimization through cation engineering of halide perovskites.

■ INTRODUCTION

Organic−inorganic halide perovskites, possessing substantial tunability in compositions and structures, have emerged as exceptionally promising candidates for optical and optoelectronic applications.[1−4] They have a chemical formula of ABX_3 where A represents an organic cation, B denotes a divalent cation, and X signifies a halogen. The electronic structures and physical properties of halide perovskites are dominated by the characteristics of the inorganic $[BX_6]^{4-}$ octahedral framework.[5] Thus far, extensive efforts have been made on the compositional tuning of B- and X-sites for materials optimization, such as achieving tunable bandgap across the entire visible spectral region.[6−9] However, the contributions of A-site cations and their interactions with the inorganic framework to the electronic structures and optical properties have long been underappreciated and remain unclear,[10,11] which thus leaves a great space for materials design and properties improvement through A-site cation engineering.

The incorporation of an oversized MHy^+ (methylhydrazinium, $CH_3NH_2NH_2^+$) has led to the development of an exotic 3D lead halide perovskite, $MHyPbBr_3$ (tolerance factor = 1.03), characterized by strong and anomalous organic−inorganic interactions.[12,13] Particularly, the Pb−N coordinate bonding[14] and N−H···Br hydrogen bonding give ordered MHy^+ cations, resulting in significant octahedral distortion within the Pb−Br inorganic framework.[15,16] Consequently, $MHyPbBr_3$ exhibits a range of unusual properties inducing strong second-harmonic-generation (SHG) activity, switchable dielectric behavior, thermochromism, and a high order−disorder transition temperature (408 K at ambient pressure).[12] The relatively strong organic−inorganic interactions in $MHyPbBr_3$ distinguish it from other lead bromide perovskites, offering exceptional opportunities to understand the role of these interactions in the structural transition and the resulting

Received: August 28, 2023
Published: October 20, 2023

https://doi.org/10.1021/jacs.3c09375
J. Am. Chem. Soc. 2023, 145, 23842−23848

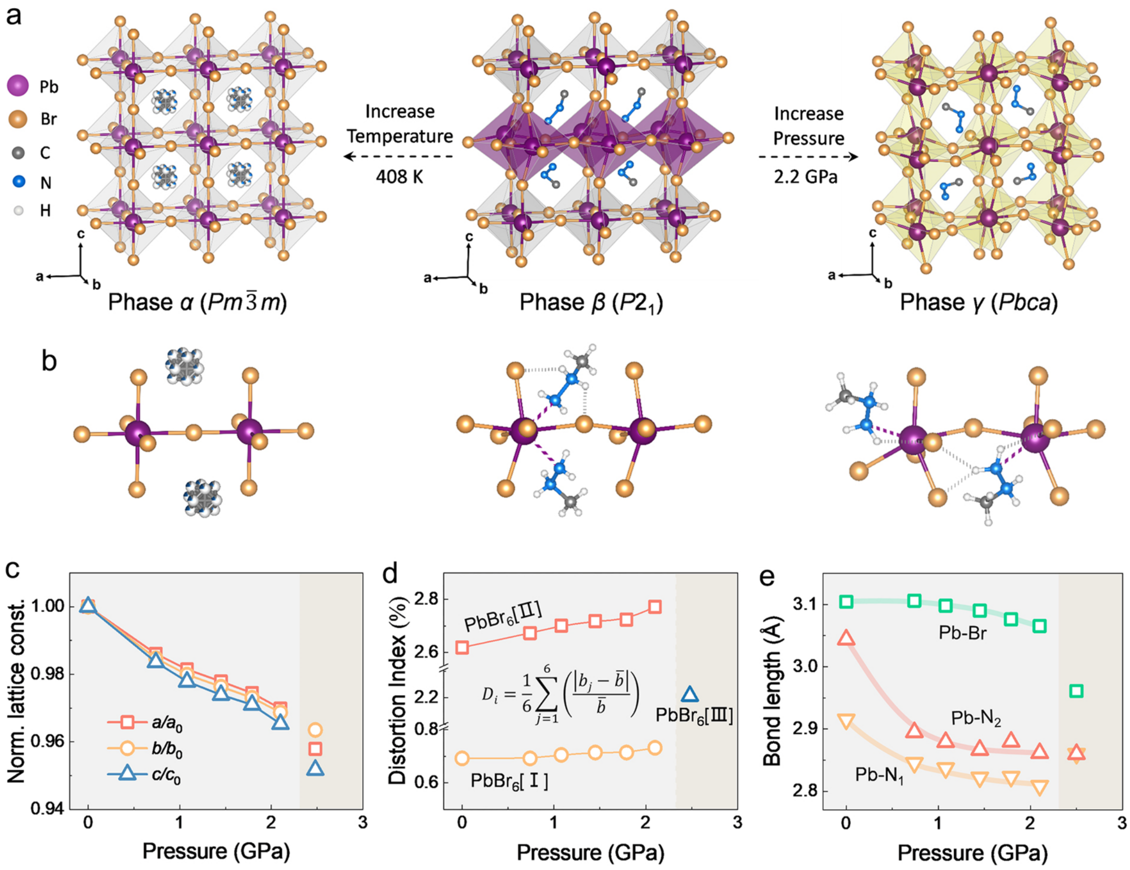

Figure 1. Structural evolution of $MHyPbBr_3$ under high pressures. (a) Crystal structures at 430 K (phase α, left panel),[12] ambient conditions (phase β, middle panel), and 2.5 GPa (phase γ, right panel). Gray, purple, and yellow colors represent low-distorted $PbBr_6$[I], high-distorted $PbBr_6$[II], and medium-distorted $PbBr_6$[III] octahedra, respectively. H atoms are hidden for clarity. (b) Schematic illustration of organic−inorganic interactions in $MHyPbBr_3$, which includes Pb−N coordinate bonds and N−H···Br hydrogen bonds. (c) Normalized lattice constants as a function of pressure. (d) Octahedral distortion index D_i as a function of pressure. (e) Pressure-dependent Pb−N bond length in the high-distorted $PbBr_6$[II] octahedron. Average length of the Pb−Br bond is shown for comparison. Left and middle panels of (a) are reproduced from *Chem. Mater.* **2020**, *32* (4), 1667. Copyright © 2022 American Chemical Society.

optical properties. Achieving this goal requires efficient tuning and diagnostic methods that enable harnessing and understanding of the organic−inorganic interactions in these hybrid halide perovskites.

Pressure, as a thermodynamic parameter, allows for the continuous modification of the lattice and electronic structures of materials without altering their chemical compositions.[17−22] Notably, the distinct pressure responses of the organic and inorganic building blocks in halide perovskites provide an avenue for manipulating the organic−inorganic interactions.[23−26] In this work, by introducing pressure to modulate the Pb−N coordinate bonding and N−H···Br hydrogen bonding in $MHyPbBr_3$, we achieve the continuous modulation of organic−inorganic interactions, which allows us to elucidate their contributions to the variations in the structure and properties of this material. Specifically, we observe an 18-fold enhancement in the SHG intensity at 1.5 GPa, along with a noteworthy increase in the order−disorder phase transition temperature from 408 K at ambient pressure to 454 K at 0.5 GPa. Furthermore, variations in the structural and physical properties have been comprehensively investigated by high-pressure diagnostics and theoretical calculations, demonstrating the direct link between the organic−inorganic interactions and the physical properties of hybrid halide perovskites.

■ RESULTS AND DISCUSSION

$MHyPbBr_3$ adopts a monoclinic structure with space group $P2_1$ (phase β) and lattice constants of a = 5.97010(10) Å, b = 11.8291(2) Å, c = 11.8582(2) Å, and β = 92.361(2)° at ambient conditions. In contrast to the randomly oriented MA^+ cations in $MAPbBr_3$, the MHy^+ cations in $MHyPbBr_3$ exhibit an ordered arrangement (Figure 1a). The specific orientation of MHy^+ cations is attributed to the strong interaction between the organic A-site cations and inorganic frameworks through Pb−N coordinate bonds and N−H···Br hydrogen bonds (as shown in Figure 1b).[15] The inorganic framework of $MHyPbBr_3$, as depicted in the middle panel of Figure 1a, is composed of two layers of octahedra stacked alternately along the *c*-axis. These octahedra include less distorted $PbBr_6$[I] octahedra shown in gray and highly distorted $PbBr_6$[II] octahedra shown in purple. As a result, the $MHyPbBr_3$ exhibits strong structural distortion, high second-harmonic intensity (1/5 KH_2PO_4),[12] and an unusually large bandgap, all of which are rarely observed in other Pb−Br perovskites (Figure S1). Furthermore, $MHyPbBr_3$ possesses an order−disorder phase transition when the temperature increased to 408 K, above which the organic−inorganic interactions were disrupted, forming a centrosymmetric structure with the $Pm\bar{3}m$ space group (phase α, left panel of Figure 1a).

https://doi.org/10.1021/jacs.3c09375
J. Am. Chem. Soc. 2023, 145, 23842−23848

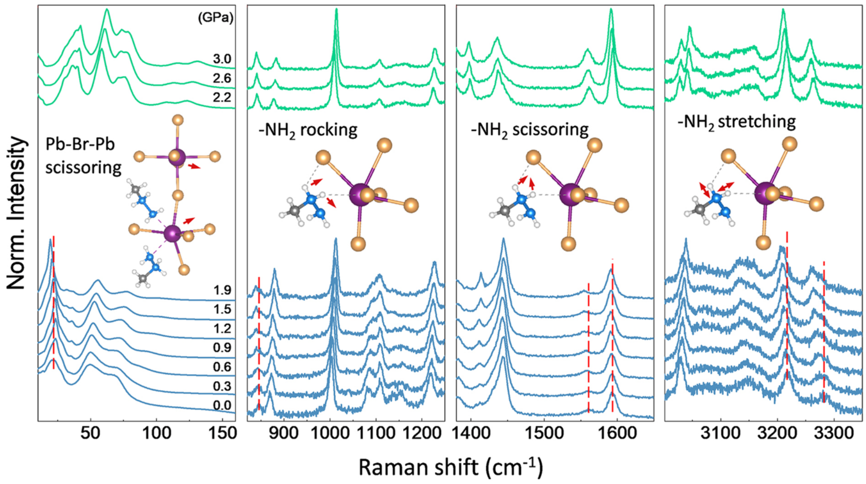

Figure 2. Raman spectra of $MHyPbBr_3$ at different pressures. Raman peaks exhibiting a redshift are marked in red, indicating the enhancement of Pb−N coordinate bonding and N−H···Br hydrogen bonding under pressure. Inset illustrates the corresponding vibration modes.

In situ single-crystal X-ray diffraction was carried out to investigate the structural evolution of $MHyPbBr_3$ under high pressures (Figure S2). Figure 1c and Table S1 show the variations of lattice constants with pressure, revealing a nearly isotropic compressibility behavior. To quantify the $PbBr_6$ octahedra distortion of $MHyPbBr_3$, we introduce the Baur distortion index D_i:

$$D_i = \frac{1}{6}\sum_{j=1}^{6}\left(\frac{|b_j - \bar{b}|}{\bar{b}}\right)$$

where b_j and $\bar{b}$ are the individual and average of Pb−Br bond length, respectively. An ideal octahedron corresponds to D_i = 0, and a higher value indicates a larger octahedral distortion.[27] As shown in Figure 1d, the D_i values for the less distorted $PbBr_6$[I] octahedra and highly distorted $PbBr_6$[II] octahedra are 0.69% and 2.62% at ambient pressure, respectively. Upon compression, the D_i values for both types of octahedra increase up to 2.1 GPa, indicating an enhanced structural distortion. We further examined the coordinate bond distance between the Pb atom in the distorted $PbBr_6$[II] octahedron and the N atoms in the two MHy^+ cations nearby, as shown in Figure 1e. Upon compression, the Pb−N_1 and Pb−N_2 distances gradually reduce from 2.92 and 3.04 Å under ambient conditions to 2.81 and 2.86 Å at 2.1 GPa, respectively. These distances are shorter than the Pb−Br bond distance, indicating a strengthened Pb−N interaction.

When the pressure exceeded 2.2 GPa, a phase transition occurred in $MHyPbBr_3$. By analyzing the single-crystal X-ray diffraction (XRD) results (Figure S3), the high-pressure phase (phase γ) of $MHyPbBr_3$ was identified as a centrosymmetric orthorhombic structure with space group *Pbca* and lattice constants of a = 11.2858(6) Å, b = 11.3973(5) Å, and c = 11.4376(17) Å. More detailed crystallographic information can be found in Table S2 of the Supporting Information. As illustrated in the right panel of Figure 1a, the high-pressure structure (phase γ) of $MHyPbBr_3$ consists of only one type of octahedron, which exhibits a medium level of distortion with D_i = 2.21% (Figure 1d). Note that the distance of the Pb−N coordinate bond increases to 2.86 Å at 2.5 GPa, which gives weaker organic−inorganic interactions and less octahedral distortion in phase γ.

To explore the evolution of local structures and organic−inorganic interactions in $MHyPbBr_3$, we conducted *in situ* Raman spectroscopy measurements, as shown in Figure 2. Generally, the low-wavenumber modes (below 200 cm^{-1}) are associated with the inorganic framework, while the modes above 280 cm^{-1} reflect the internal vibrations related to the MHy^+ cation.[12,28] At ambient conditions, the MHy^+ cation in $MHyPbBr_3$ is ordered, giving rise to clear and well-defined Raman peaks. Upon compression, most Raman peaks shift toward higher wavenumbers due to the lattice contraction. However, we note that some peaks show an opposite trend. Particularly, the peak at 22.4 cm^{-1}, which corresponds to the Pb−Br−Pb scissoring (Figure 2), exhibits a redshift and becomes sharper and stronger with increasing pressure (Figure S4). Such an anomaly is due to the enhanced Pb−N coordinate bonding.[29] The redshift can also be observed in some other modes, at the wavenumbers of 846.9, 1561.5, 3216.5, and 3268 cm^{-1}, which correspond to $-NH_2$ rocking, $-NH_2$ scissoring, N−H stretching, and N−H stretching vibrations, respectively.[28,30] These unusual redshifts indicate the enhanced N−H···Br hydrogen bonding between MHy^+ and Br^-.[31] Such enhanced hydrogen bonding together with stronger Pb−N coordinate bonding increases the organic−inorganic interactions in $MHyPbBr_3$.

The occurrence of the phase transition is also clearly reflected in the Raman spectra, as evidenced by the significant changes in the modes associated with the inorganic framework. Note that most of the Raman peaks originating from the organic cations remain well-defined but show variation, which indicates an ordered nature and altered configuration of MHy^+ after the phase transition. At high pressures, the Raman peaks influenced by hydrogen bonding persist and continue to shift toward lower wavenumbers (Figure S4c), indicating the persistence of these bondings after the phase transition.

The strong organic−inorganic interaction in $MHyPbBr_3$ leads to considerable distortion of the inorganic framework, leading to a larger bandgap (2.58 eV) compared to $MAPbBr_3$ (2.27 eV) and $FAPbBr_3$ (2.25 eV). To explore the band structure evolution under high pressure, *in situ* UV−vis absorption spectra were collected. Upon compression, the absorption edge gradually redshifts and then undergoes a sudden blueshift at 2.2 GPa (Figure 3a). The pressure-dependent bandgap of $MHyPbBr_3$ is shown in Figure 3b (left

https://doi.org/10.1021/jacs.3c09375
J. Am. Chem. Soc. 2023, 145, 23842−23848

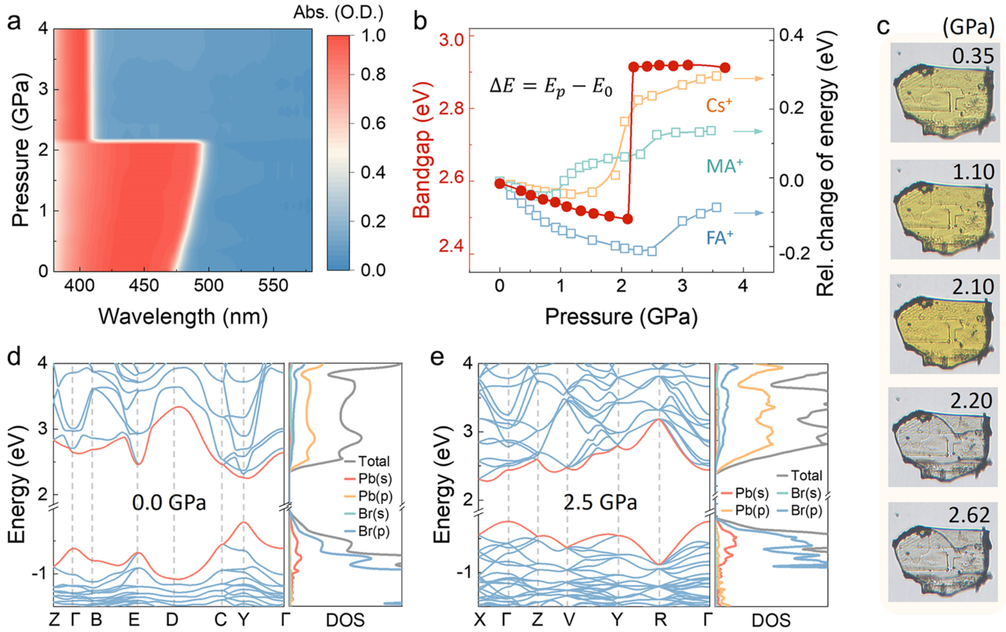

Figure 3. Optical and electronic properties of $MHyPbBr_3$ at different pressures. (a) Absorption spectra at different pressures. (b) The optical bandgap and the relative change of energy (ΔE) as a function of pressure. $\Delta E = E_p - E_0$, where the E_p and E_0 are the bandgap at specific pressure and ambient conditions, respectively. The ΔE values of $CsPbBr_3$, $MAPbBr_3$, and $FAPbBr_3$ are shown for comparison. (c) Optical images of $MHyPbBr_3$ at different pressures, where a sudden change of color from yellow to transparent is found at 2.2 GPa. The calculated electronic structures of $MHyPbBr_3$ at (d) 0.0 and (e) 2.5 GPa.

axis), and the relative changes of energy (ΔE) for $APbBr_3$ (A = Cs, MA, FA, and MHy) are displayed in the right axis. The corresponding optical absorption data of $APbBr_3$ are shown in Figure S5. As is well known, the bandgap of 3D halide perovskites is governed by the Pb−Br bond length as well as the Pb−Br octahedron distortion and tilting.[32] The decrease in bond length causes a reduction in the bandgap, whereas the distortion and tilting of the octahedra have the opposite effect. Upon compression, the bandgap of all the $APbBr_3$ perovskites initially decreases due to the shortening of the Pb−Br bond length, then exhibits an increase at the point of phase transition due to the tilting of the octahedra.[33,34] The photoluminescence (PL) spectra, displayed in Figure S6, exhibit a consistent redshift of the PL peak during compression before the phase transition, aligning with the observed variations in the bandgap.

Note that the phase-transition-induced increase in the bandgap of $MHyPbBr_3$ is 0.44 eV, which is the most dramatic and abrupt change among all $APbBr_3$ perovskites (Figure 3b). This is because the strong organic−inorganic interaction in $MHyPbBr_3$ inhibits the tilting of the Pb−Br octahedron through the steric hindrance effect.[35] Therefore, when the lattice stress surpasses a certain threshold, the original structure collapses, giving rise to a sudden octahedral tilting (as shown in Figure S7) accompanied by a large increase in the bandgap. Furthermore, the pressure-induced phase transition of $MHyPbBr_3$ is visually evident in the optical images, where the crystal color changes abruptly from yellow to transparent (Figure 3c and Figure S8).

Theoretically calculated electronic structures of $MHyPbBr_3$ at various pressures are presented in Figure 3d,e and Figure S9, where phase β and phase γ exhibit a direct and indirect bandgap nature, respectively. The states near the conduction band minimum (CBM) mainly consist of Pb-5p orbitals, and the valence band maximum (VBM) consists of Pb-6s and Br-4p antibonding orbitals. Pressure-induced shortening in the Pb−Br bond length increases the orbital overlap between Pb-6s and Br-4p, raising the VBM and thereby narrowing the bandgap. On the other hand, the orbital overlap is reduced after the phase transition due to the increased octahedra tilting, resulting in a larger bandgap in phase γ. Interestingly, we find a weak contribution of Pb-6p orbitals in the VBM, which comes from the lone-pair electrons of the N-2s orbital through Pb−N coordinate bond.[36] By integrating the density of states around the VBM at different pressures, we observe an increase in the contribution of Pb-6p orbitals in the VBM of $MHyPbBr_3$ (Figure S10), confirming the enhancement of Pb−N coordinate bonding upon compression. Additionally, the calculated pressure-dependent bandgaps are shown in Figure S11, which agrees well with the experimental results.

The pronounced structural polarization resulting from the strong organic−inorganic interactions in $MHyPbBr_3$ gives a second-order nonlinear optical effect, where the SHG intensity reaches the 1/5 value of KH_2PO_4 (KDP) at ambient conditions. The pressure-modulated organic−inorganic interactions and enhanced structural distortion offer an opportunity to further enhance the SHG response. As shown in Figure 4a, the SHG response of $MHyPbBr_3$ is significantly enhanced, reaching the maximum at around 1.5 GPa, where an 18 times gain is achieved. When the pressure exceeds 2.2 GPa, the SHG response suddenly disappears, confirming the pressure-induced phase transition from non-centrosymmetric to centrosymmetric (Figure 1a). To further analyze the relationship between crystal symmetry and SHG properties, we performed the polarization-resolved SHG measurements at various pressures in a vertical configuration (Figure 4b and Figure S12). Below the pressure corresponding to phase transition (∼2 GPa), $MHyPbBr_3$ exhibits a consistent four-lobe pattern, indicating the persistence of the same crystallographic space group in $MHyPbBr_3$ before the phase transition.[37] This suggests that

https://doi.org/10.1021/jacs.3c09375
J. Am. Chem. Soc. 2023, 145, 23842−23848

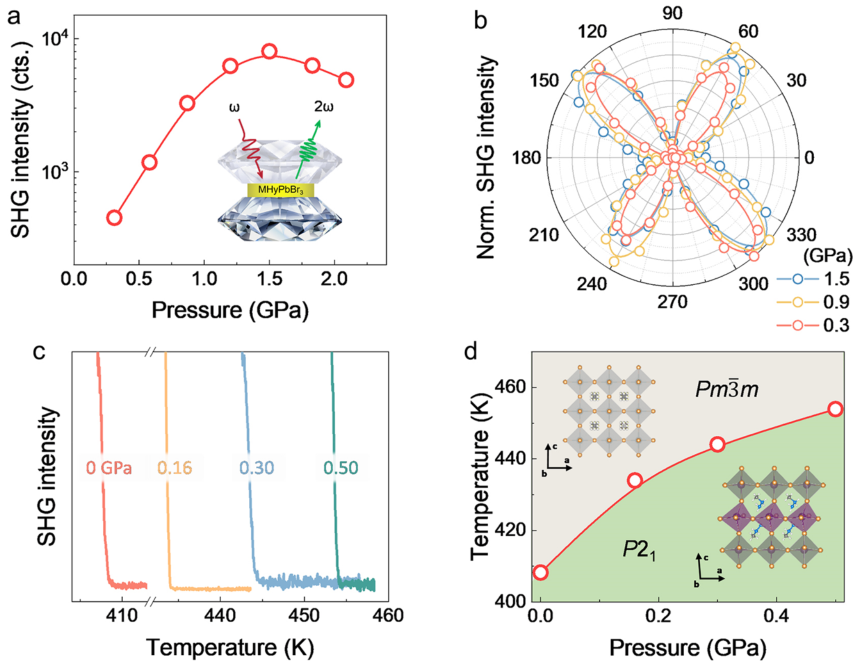

Figure 4. Pressure-dependent SHG property of $MHyPbBr_3$. (a) SHG intensity as a function of pressure at room temperature. (b) SHG polarization polar plots at selected pressures. (c) SHG intensity as a function of temperature at different pressures, where order−disorder phase transition temperature increases upon compression. (d) Temperature−pressure phase diagram of $MHyPbBr_3$, showing the nonpolarized $Pm\bar{3}m$ space group under low-pressure and high-temperature conditions and the polarized $P2_1$ space group otherwise.

the SHG enhancement in $MHyPbBr_3$ is primarily attributed to the enhanced structural distortion rather than a change in crystal symmetry.[38]

As aforementioned, the organic−inorganic interactions in $MHyPbBr_3$ could stabilize the polarized structure (phase β) up to 408 K. Above this temperature, the orientation of the MHy^+ cation becomes thermally random, leading to the disruption of the orderly organic−inorganic interaction in $MHyPbBr_3$ (Figure 1a). Consequently, the structure transforms into a typical nonpolarized $Pm\bar{3}m$ perovskite structure. We conducted temperature-dependent SHG measurements of $MHyPbBr_3$ at different pressures. As shown in Figure 4c, the critical temperature T_c gradually increases from 408 K at ambient pressure to 454 K at 0.5 GPa. The temperature−pressure phase diagram, shown in Figure 4d, illustrates that $MHyPbBr_3$ exhibits a nonpolarized $Pm\bar{3}m$ space group at the low-pressure/high-temperature region, whereas it crystallizes in a polarized $P2_1$ space group otherwise. The enhanced stability of the polarized structure in $MHyPbBr_3$ is mainly due to the strengthening of the organic−inorganic interactions under high pressure. Therefore, a higher temperature is required to overcome the energy associated with Pb−N coordinate bonding and N−H···Br hydrogen bonding, inducing randomization of the MHy^+ cations.

■ CONCLUSION

We have achieved substantial enhancement in the structural distortion and SHG response of $MHyPbBr_3$ by regulating the organic−inorganic interactions through high pressure. Compression induces strengthening of Pb−N coordinate bonding and N−H···Br hydrogen bonding in $MHyPbBr_3$ due primarily to the steric hindrance effect from the oversized MHy^+ cations. Notably, the SHG intensity of $MHyPbBr_3$ achieves a remarkable enhancement by 18-fold at 1.5 GPa and an increase in the order−disorder phase transition temperature from 408 K under ambient conditions to 454 K at the industrially achievable level of 0.5 GPa. Combined experimental data and calculation results demonstrate the stronger organic−inorganic interactions, which can be realized by introducing Pb−N coordinate bonding and increasing hydrogen bonding, leading to higher structural distortion and improved nonlinear optical properties. Our findings would lead to further studies on A-cation engineering and the understanding of organic−inorganic interactions with the polarization-related properties like ferroelectricity, piezoelectricity, and circular dichroism.

■ ASSOCIATED CONTENT

Data Availability Statement

The data that support the findings of this study are available from the corresponding author upon reasonable request.

Supporting Information

The Supporting Information is available free of charge at https://pubs.acs.org/doi/10.1021/jacs.3c09375.

Experimental details, crystallographic information, single-crystal XRD patterns, Raman peak positions, absorption spectra, photoluminescence spectra, optical images, calculated band structures, polarization-dependent polar plots (PDF)

Accession Codes

CCDC 2291223 contains the supplementary crystallographic data for this paper. These data can be obtained free of charge via www.ccdc.cam.ac.uk/data_request/cif, or by emailing data_request@ccdc.cam.ac.uk, or by contacting The Cambridge Crystallographic Data Centre, 12 Union Road, Cambridge CB2 1EZ, UK; fax: +44 1223 336033.

https://doi.org/10.1021/jacs.3c09375
J. Am. Chem. Soc. 2023, 145, 23842−23848

AUTHOR INFORMATION

Corresponding Authors

Wenge Yang – *Center for High Pressure Science and Technology Advanced Research (HPSTAR), Shanghai 201203, China;* orcid.org/0000-0001-8436-8731; Email: yangwg@hpstar.ac.cn

Xujie Lü – *Center for High Pressure Science and Technology Advanced Research (HPSTAR), Shanghai 201203, China;* orcid.org/0000-0001-8402-7160; Email: xujie.lu@hpstar.ac.cn

Authors

Yuhong Mao – *Center for High Pressure Science and Technology Advanced Research (HPSTAR), Shanghai 201203, China*

Songhao Guo – *Center for High Pressure Science and Technology Advanced Research (HPSTAR), Shanghai 201203, China;* orcid.org/0000-0003-0570-0164

Xu Huang – *Beijing National Laboratory for Molecular Science, College of Chemistry and Molecular Engineering, Peking University, Beijing 100871, China*

Kejun Bu – *Center for High Pressure Science and Technology Advanced Research (HPSTAR), Shanghai 201203, China;* orcid.org/0000-0002-1466-2764

Zhongyang Li – *Center for High Pressure Science and Technology Advanced Research (HPSTAR), Shanghai 201203, China*

Phuong Q. H. Nguyen – *Hawaii Institute of Geophysics and Planetology, School of Ocean and Earth Science and Technology, University of Hawaii at Manoa, Honolulu, Hawaii 96822, United States*

Gang Liu – *Center for High Pressure Science and Technology Advanced Research (HPSTAR), Shanghai 201203, China*

Qingyang Hu – *Center for High Pressure Science and Technology Advanced Research (HPSTAR), Shanghai 201203, China;* orcid.org/0000-0002-2742-3017

Dongzhou Zhang – *Hawaii Institute of Geophysics and Planetology, School of Ocean and Earth Science and Technology, University of Hawaii at Manoa, Honolulu, Hawaii 96822, United States;* orcid.org/0000-0002-6679-892X

Yongping Fu – *Beijing National Laboratory for Molecular Science, College of Chemistry and Molecular Engineering, Peking University, Beijing 100871, China;* orcid.org/0000-0003-3362-2474

Complete contact information is available at: https://pubs.acs.org/10.1021/jacs.3c09375

Author Contributions

#Y.M. and S.G. contributed equally to this work.

Notes

The authors declare no competing financial interest.

ACKNOWLEDGMENTS

This work is supported by the National Nature Science Foundation of China (NSFC) (Grant Nos. 22275004, U1930401, 52103353, and 22271006), Shanghai Science and Technology Committee (No. 22JC1410300), and Shanghai Key Laboratory of Novel Extreme Condition Materials (No. 22dz2260800). Q.H. is supported by the National Natural Science Foundation of China (No. 17N1051-0213). Portions of this work were performed at GeoSoilEnviroCARS (The University of Chicago, Sector 13), Advanced Photon Source (APS), Argonne National Laboratory. GeoSoilEnviroCARS is supported by the National Science Foundation – Earth Sciences (EAR-1634415). This research used resources of the Advanced Photon Source, a U.S. Department of Energy (DOE) Office of Science User Facility operated for the DOE Office of Science by Argonne National Laboratory under Contract No. DE-AC02-06CH11357. X. Huang acknowledges the National Training Program of Innovation for Undergraduates.

REFERENCES

(1) Huang, J.; Yuan, Y.; Shao, Y.; Yan, Y. Understanding the physical properties of hybrid perovskites for photovoltaic applications. *Nat. Rev. Mater.* **2017**, *2*, 17042.

(2) Fu, Y.; Zhu, H.; Chen, J.; Hautzinger, M. P.; Zhu, X. Y.; Jin, S. Metal halide perovskite nanostructures for optoelectronic applications and the study of physical properties. *Nat. Rev. Mater.* **2019**, *4*, 169–188.

(3) Gratzel, M. The light and shade of perovskite solar cells. *Nat. Mater.* **2014**, *13*, 838–42.

(4) Han, T.-H.; Jang, K. Y.; Dong, Y.; Friend, R. H.; Sargent, E. H.; Lee, T.-W. A roadmap for the commercialization of perovskite light emitters. *Nat. Rev. Mater.* **2022**, *7*, 757–777.

(5) Chouhan, L.; Ghimire, S.; Subrahmanyam, C.; Miyasaka, T.; Biju, V. Synthesis, optoelectronic properties and applications of halide perovskites. *Chem. Soc. Rev.* **2020**, *49*, 2869–2885.

(6) Smith, M. D.; Connor, B. A.; Karunadasa, H. I. Tuning the Luminescence of Layered Halide Perovskites. *Chem. Rev.* **2019**, *119*, 3104–3139.

(7) Zhang, F.; Zhong, H.; Chen, C.; Wu, X. G.; Hu, X.; Huang, H.; Han, J.; Zou, B.; Dong, Y. Brightly Luminescent and Color-Tunable Colloidal $CH_3NH_3PbX_3$ (X = Br, I, Cl) Quantum Dots: Potential Alternatives for Display Technology. *ACS Nano* **2015**, *9*, 4533–42.

(8) Kovalenko, M. V.; Protesescu, L.; Bodnarchuk, M. I. Properties and potential optoelectronic applications of lead halide perovskite nanocrystals. *Science* **2017**, *358*, 745–750.

(9) Zhu, H.; Fu, Y.; Meng, F.; Wu, X.; Gong, Z.; Ding, Q.; Gustafsson, M. V.; Trinh, M. T.; Jin, S.; Zhu, X. Y. Lead halide perovskite nanowire lasers with low lasing thresholds and high quality factors. *Nat. Mater.* **2015**, *14*, 636–42.

(10) Svane, K. L.; Forse, A. C.; Grey, C. P.; Kieslich, G.; Cheetham, A. K.; Walsh, A.; Butler, K. T. How Strong Is the Hydrogen Bond in Hybrid Perovskites? *J. Phys. Chem. Lett.* **2017**, *8*, 6154–6159.

(11) Lee, J. W.; Tan, S.; Seok, S. I.; Yang, Y.; Park, N. G. Rethinking the A cation in halide perovskites. *Science* **2022**, *375*, eabj1186.

(12) Mączka, M.; Ptak, M.; Gągor, A.; Stefańska, D.; Zaręba, J. K.; Sieradzki, A. Methylhydrazinium Lead Bromide: Noncentrosymmetric Three-Dimensional Perovskite with Exceptionally Large Framework Distortion and Green Photoluminescence. *Chem. Mater.* **2020**, *32*, 1667–1673.

(13) Fu, Y.; Hautzinger, M. P.; Luo, Z.; Wang, F.; Pan, D.; Aristov, M. M.; Guzei, I. A.; Pan, A.; Zhu, X.; Jin, S. Incorporating Large A Cations into Lead Iodide Perovskite Cages: Relaxed Goldschmidt Tolerance Factor and Impact on Exciton-Phonon Interaction. *ACS Cent. Sci.* **2019**, *5*, 1377–1386.

(14) Mączka, M.; Sobczak, S.; Ratajczyk, P.; Leite, F. F.; Paraguassu, W.; Dybała, F.; Herman, A. P.; Kudrawiec, R.; Katrusiak, A. Pressure-Driven Phase Transition in Two-Dimensional Perovskite MHy_2PbBr_4. *Chem. Mater.* **2022**, *34*, 7867–7877.

(15) Drozdowski, D.; Gągor, A.; Stefańska, D.; Zaręba, J. K.; Fedoruk, K.; Mączka, M.; Sieradzki, A. Three-Dimensional Methylhydrazinium Lead Halide Perovskites: Structural Changes and Effects on Dielectric, Linear, and Nonlinear Optical Properties Entailed by the Halide Tuning. *J. Phys. Chem. C* **2022**, *126*, 1600–1610.

(16) Huang, X.; Li, X.; Tao, Y.; Guo, S.; Gu, J.; Hong, H.; Yao, Y.; Guan, Y.; Gao, Y.; Li, C.; Lu, X.; Fu, Y. Understanding Electron-Phonon Interactions in 3D Lead Halide Perovskites from the

Stereochemical Expression of $6s^2$ Lone Pairs. *J. Am. Chem. Soc.* **2022**, *144*, 12247−12260.

(17) Drozdov, A. P.; Kong, P. P.; Minkov, V. S.; Besedin, S. P.; Kuzovnikov, M. A.; Mozaffari, S.; Balicas, L.; Balakirev, F. F.; Graf, D. E.; Prakapenka, V. B.; Greenberg, E.; Knyazev, D. A.; Tkacz, M.; Eremets, M. I. Superconductivity at 250 K in lanthanum hydride under high pressures. *Nature* **2019**, *569*, 528−531.

(18) Guo, S.; Bu, K.; Li, J.; Hu, Q.; Luo, H.; He, Y.; Wu, Y.; Zhang, D.; Zhao, Y.; Yang, W.; Kanatzidis, M. G.; Lu, X. Enhanced Photocurrent of All-Inorganic Two-Dimensional Perovskite $Cs_2PbI_2Cl_2$ via Pressure-Regulated Excitonic Features. *J. Am. Chem. Soc.* **2021**, *143*, 2545−2551.

(19) Lin, J.; Chen, H.; Gao, Y.; Cai, Y.; Jin, J.; Etman, A. S.; Kang, J.; Lei, T.; Lin, Z.; Folgueras, M. C.; Quan, L. N.; Kong, Q.; Sherburne, M.; Asta, M.; Sun, J.; Toney, M. F.; Wu, J.; Yang, P. Pressure-induced semiconductor-to-metal phase transition of a charge-ordered indium halide perovskite. *Proc. Natl. Acad. Sci. U.S.A.* **2019**, *116*, 23404−23409.

(20) Xiao, T.; Nagaoka, Y.; Wang, X.; Jiang, T.; LaMontagne, D.; Zhang, Q.; Cao, C.; Diao, X.; Qiu, J.; Lu, Y.; Wang, Z.; Cao, Y. C. Nanocrystals with metastable high-pressure phases under ambient conditions. *Science* **2022**, *377*, 870−874.

(21) Mao, H.-K.; Chen, B.; Gou, H.; Li, K.; Liu, J.; Wang, L.; Xiao, H.; Yang, W. 2020—Transformative science in the pressure dimension. *Matter Radiat. Extremes* **2021**, *6*, No. 013001.

(22) Ma, Z.; Xiao, G.; Zou, B. Step forward to light up the future: pressure-induced emission. *Sci. Bull.* **2023**, *68*, 1588−1590.

(23) Chen, M.; Guo, S.; Bu, K.; Lee, S.; Luo, H.; Wang, Y.; Liu, B.; Yan, Z.; Dong, H.; Yang, W.; Ma, B.; Lü, X. Pressure-induced robust emission in a zero-dimensional hybrid metal halide $(C_9NH_{20})_6Pb_3Br_{12}$. *Matter Radiat. Extremes* **2021**, *6*, No. 058401.

(24) Guo, S.; Li, Y.; Mao, Y.; Tao, W.; Bu, K.; Fu, T.; Zhao, C.; Luo, H.; Hu, Q.; Zhu, H.; Shi, E.; Yang, W.; Dou, L.; Lu, X. Reconfiguring band-edge states and charge distribution of organic semiconductor-incorporated 2D perovskites via pressure gating. *Sci. Adv.* **2022**, *8*, eadd1984.

(25) Li, M.; Liu, T.; Wang, Y.; Yang, W.; Lü, X. Pressure responses of halide perovskites with various compositions, dimensionalities, and morphologies. *Matter Radiat. Extremes* **2020**, *5*, No. 018201.

(26) Morteza Najarian, A.; Dinic, F.; Chen, H.; Sabatini, R.; Zheng, C.; Lough, A.; Maris, T.; Saidaminov, M. I.; García de Arquer, F. P.; Voznyy, O.; Hoogland, S.; Sargent, E. H. Homomeric chains of intermolecular bonds scaffold octahedral germanium perovskites. *Nature* **2023**, *620*, 328−335.

(27) Fu, Y.; Jin, S.; Zhu, X. Y. Stereochemical expression of ns^2 electron pairs in metal halide perovskites. *Nat. Rev. Chem.* **2021**, *5*, 838−852.

(28) Mączka, M.; Ptak, M.; Vasconcelos, D. L. M.; Giriunas, L.; Freire, P. T. C.; Bertmer, M.; Banys, J.; Simenas, M. NMR and Raman Scattering Studies of Temperature- and Pressure-Driven Phase Transitions in $CH_3NH_2NH_2PbCl_3$ Perovskite. *J. Phys. Chem. C* **2020**, *124*, 26999−27008.

(29) Zhang, H.; Wu, Y.; Shen, C.; Li, E.; Yan, C.; Zhang, W.; Tian, H.; Han, L.; Zhu, W. H. Efficient and Stable Chemical Passivation on Perovskite Surface via Bidentate Anchoring. *Adv. Energy Mater.* **2019**, *9*, 1803573.

(30) Mączka, M.; Gagor, A.; Zaręba, J. K.; Stefanska, D.; Drozd, M.; Balciunas, S.; Šimėnas, M.; Banys, J.; Sieradzki, A. Three-Dimensional Perovskite Methylhydrazinium Lead Chloride with Two Polar Phases and Unusual Second-Harmonic Generation Bistability above Room Temperature. *Chem. Mater.* **2020**, *32*, 4072−4082.

(31) Yin, T.; Fang, Y.; Fan, X.; Zhang, B.; Kuo, J.-L.; White, T. J.; Chow, G. M.; Yan, J.; Shen, Z. X. Hydrogen-Bonding Evolution during the Polymorphic Transformations in $CH_3NH_3PbBr_3$: Experiment and Theory. *Chem. Mater.* **2017**, *29*, 5974−5981.

(32) Zhang, R.; Cai, W.; Bi, T.; Zarifi, N.; Terpstra, T.; Zhang, C.; Verdeny, Z. V.; Zurek, E.; Deemyad, S. Effects of Nonhydrostatic Stress on Structural and Optoelectronic Properties of Methylammonium Lead Bromide Perovskite. *J. Phys. Chem. Lett.* **2017**, *8*, 3457−3465.

(33) Wang, L.; Wang, K.; Zou, B. Pressure-Induced Structural and Optical Properties of Organometal Halide Perovskite-Based Formamidinium Lead Bromide. *J. Phys. Chem. Lett.* **2016**, *7*, 2556−62.

(34) Li, X.; Cuthriell, S. A.; Bergonzoni, A.; Dong, H.; Traoré, B.; Stoumpos, C. C.; Guo, P.; Even, J.; Katan, C.; Schaller, R. D.; Kanatzidis, M. G. Expanding the Cage of 2D Bromide Perovskites by Large A-Site Cations. *Chem. Mater.* **2022**, *34*, 1132−1142.

(35) Zhao, D.; Cong, M.; Liu, Z.; Ma, Z.; Wang, K.; Xiao, G.; Zou, B. Steric hindrance effects on the retention of pressure-induced emission toward scintillators. *Cell Rep. Phys. Sci.* **2023**, *4*, 101445.

(36) Li, R.; Wang, Z.; Zhu, T.; Ye, H.; Wu, J.; Liu, X.; Luo, J. Stereochemically Active Lone Pair Induced Polar Tri-layered Perovskite for Record-Performance Polarized Photodetection. *Angew. Chem., Int. Ed.* **2023**, No. e202308445.

(37) Bu, K.; Fu, T.; Du, Z.; Feng, X.; Wang, D.; Li, Z.; Guo, S.; Sun, Z.; Luo, H.; Liu, G.; Ding, Y.; Zhai, T.; Li, Q.; Lü, X. Enhanced Second-Harmonic Generation of van der Waals CuInP2S6 via Pressure-Regulated Cationic Displacement. *Chem. Mater.* **2023**, *35*, 242−250.

(38) Fu, T.; Bu, K.; Sun, X.; Wang, D.; Feng, X.; Guo, S.; Sun, Z.; Fang, Y.; Hu, Q.; Ding, Y.; Zhai, T.; Huang, F.; Lu, X. Manipulating Peierls Distortion in van der Waals $NbOX_2$ Maximizes Second-Harmonic Generation. *J. Am. Chem. Soc.* **2023**, *145*, 16828−16834.

https://doi.org/10.1021/jacs.3c09375
J. Am. Chem. Soc. 2023, 145, 23842−23848